Novel hybrid polymer nanocomposites for biological and Environmental applications

S.Siva[a], S.Sudharsan[b], R. Sakthivadivel[d],M.Jayalakshmi[a], R.Mahalakshmi[a] and R.SayeeKannan[c*]

[a]*Department of Chemistry, Noble College of Arts and Science For Women, Palavanatham -626004, India.*
[b]*Department of Chemistry, Mohamed Sathak College of Arts and Science, Chennai-600119, India.*
[c] *PG Research & Department of chemistry, Thiagarajar College, Madurai-625 009, India.*
[d]*PG Research & Department of Chemistry Madura College, Maurai -625 011, India.*

Abstract:

The current study aims at a simple and eco-friendly biosynthesis of AgNPs using Cyperus rotundus grass extract (CRGE) as reducing agent without involving chemical agents associated with environmental toxicity. Polymer nanocomposites (RFR-AgNPs) were then built by immobilizing AgNPs onto a macroporous Resorcinol-formaldehyde resin (RFR) by polycondensation method via formaldehyde performs as a cross-linking agent for sensing and selective sequestration of mercury from polluted aqueous medium in the presence of alkali and alkaline earth metals. RFR was chosen as a hold material principally as the potential Donnan membrane effect enforced through immobilized minus charged sulphonic acid groups linked to the RFR pattern, which developed the extraction of Hg(II) from polluted aqueous medium by the infused AgNPs. The RFR-AgNPs exerted a signficant Hg (II) adsorption and prominent antibacterial efficacy against the water-borne diseases causing gram-negative (Escherichia coli, Salmonella typhi) and gram-positive (Bacillus subtilis and Staphylococcus aureus) bacteria. The polymer nanocomposites have great potential for utilization in the prevention and treatment of microbial diseases and heavy metals pollution for environmental applications. The Hg^{2+} adsorption on RFR AgNPs can be remarkably expressed with the Langmuir adsorption isotherm model by R^2 value 0.9957. The Hg^{2+} adsorption on RFR-AgNPs adopted with the pseudo second order kinetics model by R^2 value 0.9742. To explore the data, Weber–Morris intraparticle diffusion model was exploited. The thermodynamic factors (ΔH^O, ΔS^O & ΔG^O) for the adsorption process were also calculated. A succession of column experiments in the presence of opposing ions (e.g. Ca^{2+}, Mg^{2+}, and Na^+) were done for detect the breakthrough curves. The spent ion exchanger beads are readily to effective regeneration with the 10% (w/w) NaCl solution for echoed use without whatever substantial power loss.

Keywords: *Zerovalent silver nanoparticles; Resorcinol-formaldehyde resin; polymer nanocomposites; antibacterial efficacy; mercury (II) removal.*

I. Introduction

The progress of industries has accelerated the contamination of water bodies such as oceans, lakes, rivers and groundwater with heavy metal ions is a universal environmental problem. The existence of heavy metals in water bodies has raised anxiety towards human beings, animals and plants. Among the heavy metals, mercury well-known as a type of extremely poisonous and non-biodegradable metal also possibly will cause health hazard while even at very low concentration in water [1]. Hence the removal of mercury from effluents has been a major trepidation in mainly industries because of monetary and ecological aspects. Several efficient methods for mercury removal from the aqueous solution and wastewater are continuously followed such as ion-exchange, membrane filtration, reverse osmosis, chemical precipitation, adsorption and electrochemical treatment [2]. Among these techniques, ion-exchange is a better technique with numerous advantages related with high removal capacity, cheap and superior renewability. Among the materials utilized in this technique, synthetic polymeric ion exchangers are universally chosen as they are effective and economical. As a result they are unable to entrap the heavy metals to meet the standard regulation by latest strict rules mainly in the occurrence of other opposing ions (e.g. Ca^{2+}, Mg^{2+}, and Na^+). Consequently, it demands the improvement of innovative definite adsorbents for removing heavy metal ions selectively from waste water in the presence of rival ions. Formerly, we have been applied the AgNPs (zero valent metal) as exact adsorbents for removing heavy metals from wastewater as well as improved ecological quality [3]. However, these nanoparticles are commonly show as fine or ultrafine particles [4] and cannot be applied solely

in fixed-bed or any flow-through systems due to the severe pressure drop and meager mechanical strength. To overcome the technological bottlenecks, hybrid adsorbents were then developed by impregnating these nanoparticles within the schematic important porous materials like activated carbon [5] and porous polymer [6]. Among these, the synthetic porous polymer is principally selective due to their expedient pore space, superior mechanical strength and also the potential Donnan membrane effect applied by the immobilized negatively charged sulfonic acid groups bound to the polymer matrix, where objective metal ions would be subjugated to preconcentration and incursion improvement prior to their efficient separatism by the impregnated nanoparticles [7]. Previously, we have been designed hybrid adsorbents (PFR-AgNPs) by encapsulating AgNPs within a macroporous phenol-formaldehyde polymer matrix for the sensing and efficient removing of Co (II) from aqueous medium through inner-sphere mechanism depends on potential donnan membrane principle [8]. The server materials developed permeableness in flow-through schemes devoid of manipulating the adsorption performances of the AgNPs as well as consequential hybrid adsorbents reveal latent application in heavy metals extraction. So far, Resorcinol-formaldehyde polymer integrated with AgNPs (RFR-AgNPs) based on potential donnan membrane principle was not researched for effective removing of heavy metal ions. In the current study we urbanized a RFR-AgNPs by impregnating AgNPs within a macroporous resorcinol-formaldehyde cation exchanger for the effectual extracting of mercury from aqueous medium in the presence of co-existing ions. Moreover, AgNPs contain high surface area so they are extremely reactive species at nanometer scale as well as they have been a subject for a lot of antibacterial applications [9]. since sulfur and phosphorous are detected in large quantity all over cell membrane, AgNPs react with sulfur- incorporating proteins interior or exterior of the cell membrane, which in order affects cell capability [10]. one more assumption suggested that Ag^+ ions from AgNPs can interact with phosphorous medieties in DNA ensuing in deactivation of DNA replication and can react with sulfur- comprising proteins to bottle up enzyme roles [11]. As a result, the AgNPs are impregnated into a variety of matrix for instance macro porous polymer matrix, activated carbon, wound dressing materials and textiles. In this research work, eco-friendly biological reduction method exploited to synthesize AgNPs in a non-hazardous (plant extract) solution using CRGE as per literature [12] and then the AgNPs are immediately loaded on RFR to synthesize RFR-AgNPs through polycondensation method [13]. As well, we screened the biological characteristics of the RFR-AgNPs, RFR and AgNPs by targeting few harmful water borne diseases inducing bacterial strains *viz*., Escherichia coli, Salmonella typhi (Gram-negative), Bacillus subtilis and Staphylococcus aureus (Gram-positive) and develops the selective Hg (II) adsorption of the RFR in the presence of competing alkali and alkaline earth metals (e.g. Ca^{2+}, Mg^{2+}, and Na^+) by loading the AgNPs. Moreover, the adsorption kinetics and isotherms were as well conferred. To find out the breakthrough curves in the existence of concurrent ions (e.g. Ca^{2+}, Mg^{2+}, and Na^+), A cycle of column experiments were completed. The regenerant employed for regeneration of the RFR-AgNPs was 10% (w/w) NaCl.

II. EXPERIMENTAL

A. Materials

Cyperus rotundus grass (C.rotundus) were locally collected and cleaned before use. Resorcinol and formaldehyde used in the current study were Fischer reagents (India). LR grade (purity: 98.3%) of concentrated Sulphuric acid (Sp.gr. = 1.82) was used. AR grade SD fine silver nitrate ($AgNO_3$) was purchased and its 0.1 M solution was prepared in stock and diluted to 1 mM solution. All the microorganisms were procured from Microbial Type Culture Collection, Chandigarh, India. All other chemicals and reagents were of chemically pure grade (AnalaR) procured from SD Fine Chemicals, India. Stock solutions of the RFR-AgNPs, the RFR and the AgNPs dispersed in deionized water were prepared.

B. Methods

a) Synthesis of RFR-AgNPs

Resorcinol (10g) and Con. H_2SO_4 (11.5mL) were blended gradually through constant stirring and kept overnight [14]. 1% and 0% (w/w) of AgNPs were introduced separately with the Resorcinol sulphonic acid as well as symbolize the samples marked as RFR-AgNPs and RFR. The mixtures were polymerized with formaldehyde (12.5mL) at 110^OC and cured at this temperature for 3 h to yield a dark brown chunky mass which was ground, washed, dried and sieved (250– 300μm) using Jayant sieves (India) and preserved for characterization [15].

C. Characterization of the samples

The existence of AgNPs in the RFR-AgNPs was supported with UV–Vis spectrophotometer (UV-1800 SHIMADZU spectrophotometer) at the wavelength of 300-800 nm. FT-IR (SHIMADZU MODEL FT-IR

spectrometer) spectra was used to the study the before and after Hg (II) adsorption on resins using the IR-grade KBr pellets in the ratio of 1:200 at the wave number ranging from 400 to 4000 cm^{-1}. SEM (Vega3 Tescan SEM instrument) was used to examine the surface morphology of free and Hg (II) loaded resins. EDX (Bruker machine) was used to analyze the elemental composition of free and Hg (II) loaded resins. TGA and DTA analyzer (SII MODEL 6000 thermal analyzer) was used to study the thermal degradation of the free and Hg (II) treated resins.

D. Heavy metal extraction experiment through batch analysis:

These experiment was done by adding a ideal quantity of RFR and RFR-AgNPs resin in 250 mL glass bottles alone holding Hg (II) solutions of respective concentrations (30-150 mg/L). The glass bottles were placed into a remi rotator water bath shaking machine at constant temperature (303K) and then shaken with the 200 rpm to acquire the equilibrium. The shakeup era was altered from 10 to 50 min in the following stages alike 10, 20, 30, 40 and 50 min at 303K to obtain the equilibrium. The rest concentration of the Hg (II) ions in the aqueous solution was found out with standard titration techniques as per the literature [16]. Adsorption capacity ($\mathbf{q_e}$) was determined with the following equation.

$$\mathbf{q_e = (C_o - C_e) \times V / M} \quad \text{---------- (1)}$$

Where q_e is the equilibrium adsorption capacity (mg g^{-1}), C_e is the concentration of metal ion (mg L^{-1}) at equilibrium, V is the volume of solution (L) and M is the weight (g) of adsorbent.

E. Column adsorption studies

The fixed-bed Column experiments were carried out in a glass column with 2.0 cm internal diameter and 35cm height and packed with 2 cm (3.5g) of RFR and RFR-AgNPs were packed into two separate columns. The bed volume of the column is 6.28 cm^3. Then the glass wool beads were added to improve the flow circulation. Hg (II) ions solution (initial concentration= 2mg/L) and other opposing ions were utilized as influent with high concentration than the objective heavy metals and fed through the column at a constant flow rate of 5 mL/min in down-flow mode. The samplings in the exit were taken at the predetermined period gaps and the concentrations of Hg (II) ions were found out with the EDTA titration techniques. Breakthrough curves were evaluated through plotting volume of the inlet against the proportion of Hg (II) ions concentrations in the outlet across the column for the extraction of Hg (II) from aqueous medium. In the present work, desorption study was done with the 10% (w/w) NaCl as the eluting agent.

$$\textbf{\% of Regeneration} = \frac{\text{Amount of metal ions desorbed}}{\text{Amount of metal ions adsorbed}} \times 100 \quad \text{--------- (1)}$$

F. Thermodynamics of ion-exchanger

The thermodynamic factors such as Gibb's free energy (ΔG^O), enthalphy (ΔH^O), and entrophy (ΔS^O) changes for the ion-exchange process were determined with Van't Hoff isotherm, Van't Hoff and Gibbs Helmholtz equation.

G. In vitro Antibacterial Studies

In order to explore their biological applications, the RFR-AgNPs, the RFR and the AgNPs were tested for *in vitro* antibacterial activity against few pathogenic bacterial strains. The *in vitro* antibacterial activity was carried out against *Escherichia coli*, *Salmonella typhi* (Gram-negative), *Bacillus subtilis* and *Staphylococcus aureus* (Gram-positive) by paper disk method, using nutrient agar as the medium and ciprofloxacin as the standard (200 µg/disk). Each strain was swabbed uniformly on the plates using sterile cotton swabs. For the measurement of the activity, the samples were coated in punched disks (diameter) of 6 mm, and the activity was determined using a modified agar diffusion assay (disk test). The presence of clear zone around the paper disk on the plate medium was recorded as an indication of inhibition against the bacterial species. After incubation at 37 °C, the different levels of zone of inhibition of bacteria (for 48 h) were determined [17].

III. Results and discussion

A. UV–Vis, FT-IR, SEM, SEM-EDX, XRD, AFM, TGA and DTA analysis:

Prior reports exposed that the spherical silver nanoparticles exhibit absorption bands about 400–440 nm in the UV-Visible spectrophotometer [18]. UV–Visible spectra indicated that the broad surface plasmon resonance 425 nm in Fig.1a, this is signifying the presence of particles with a broad size distribution and the existence of silver

particles in the RFR-AgNPs. Then the schematic structure of the RFR-AgNPs was shown in fig.1b, the sulfonate functional group and AgNPs have potential active sites for the withholding of Hg (II) from aqueous media, which were found out and discussed with additional information's in the subsequent sections.

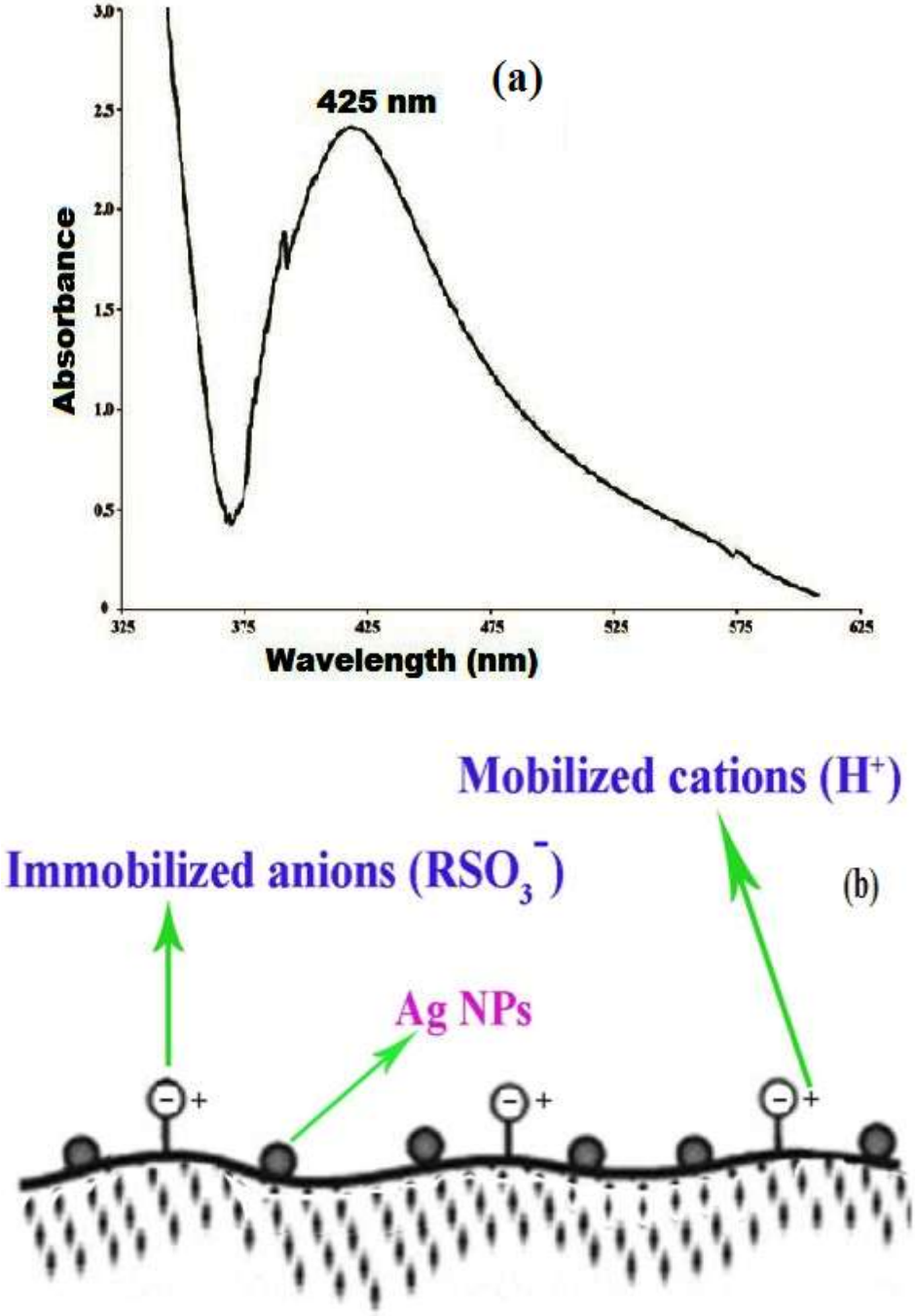

Fig.1 UV-Visible spectra (a) & schematic structure (b) of the RFR-AgNPs

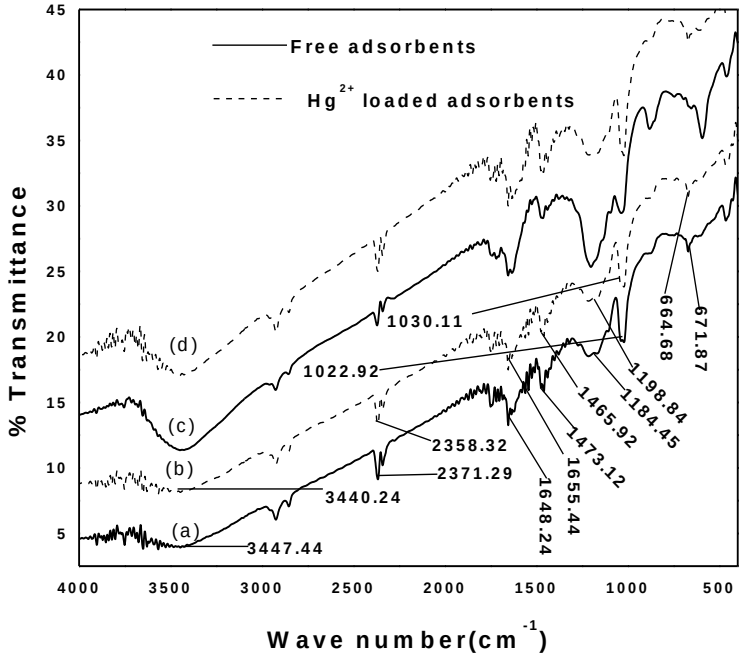

Fig.2 IR spectra of the free (a and c) & Hg^{2+} loaded (b and d) RFR & RFR–AgNPs

The FT-IR spectra of the free and Hg^{2+} loded adsorbents were shown in Fig.2a, 2b, 2c, 2d and table 1. These indicated a shift or disappear in wave number of dominant peaks related with the loaded metal and confirmed the metal binding process occurring at the exterior of resin. This information gives confirmation that the functional groups of SO_3^- are involved in binding the Hg (II) ions onto the ion exchange resins [19].

As observed from SEM images (3a, 3b, 3c & 3d), a visible change of the surface morphology in the Hg (II) loaded RFR and RFR- AgNPs exhibited that the adsorption of Hg (II) ions has happened on the resin.

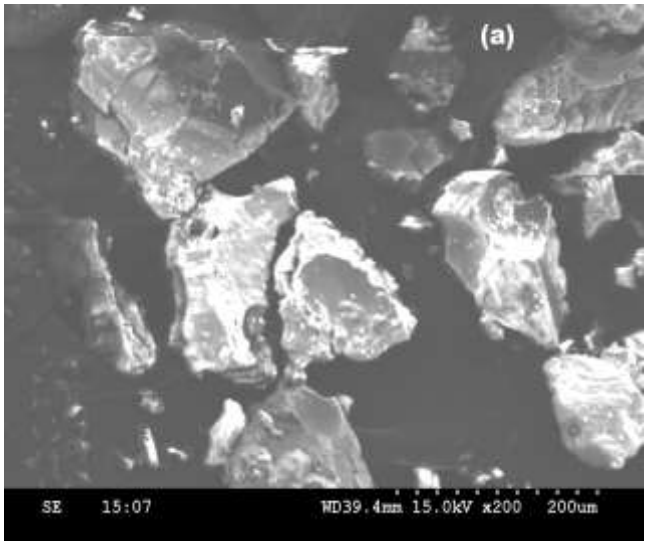

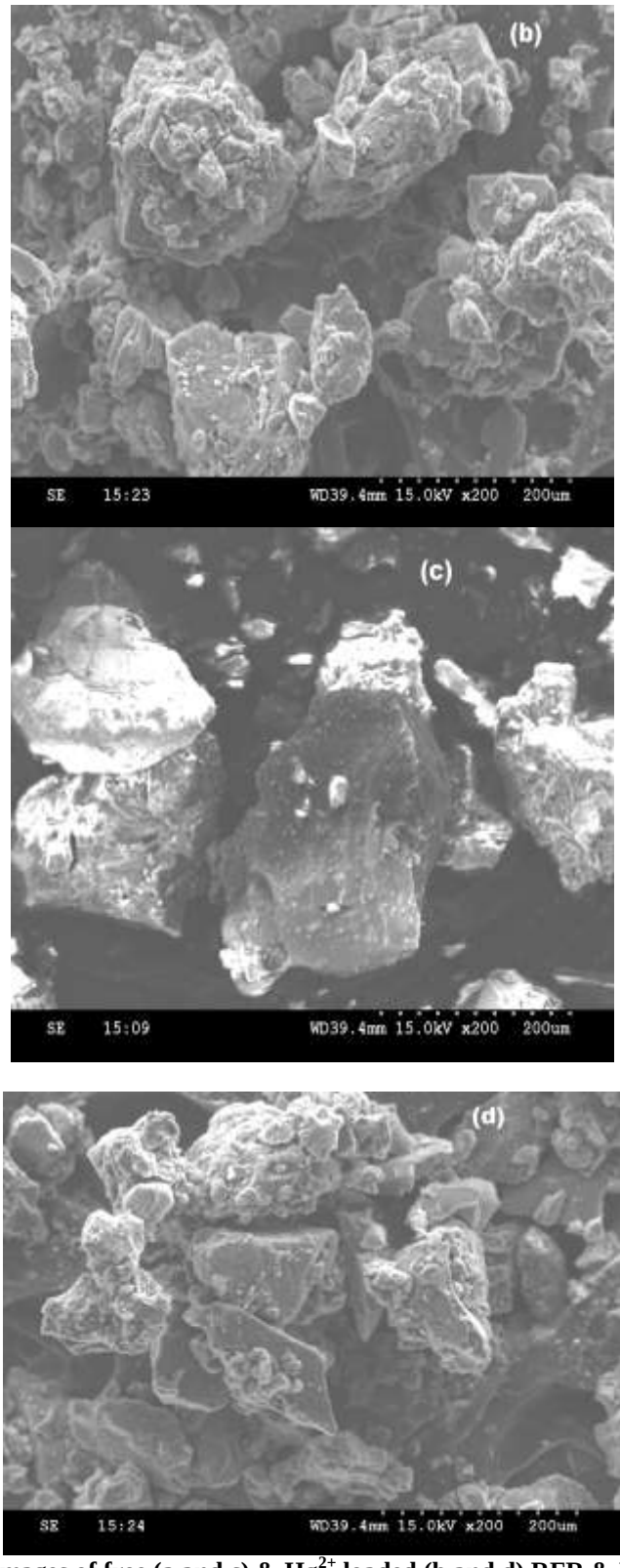

Fig.3 SEM images of free (a and c) & Hg^{2+} loaded (b and d) RFR & RFR-AgNPs

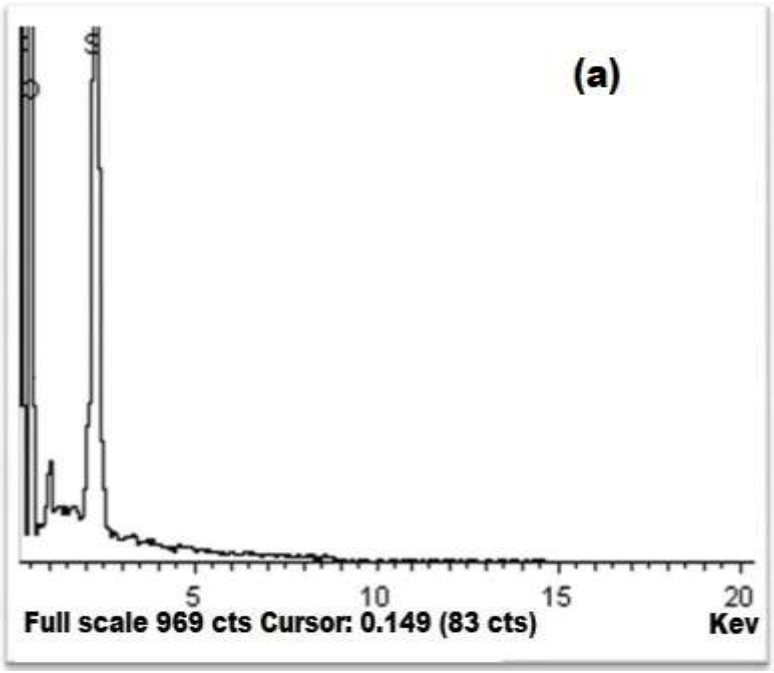
(a)
5
10
15
20
Full scale 969 cts Cursor: 0.149 (83 cts)
Kev

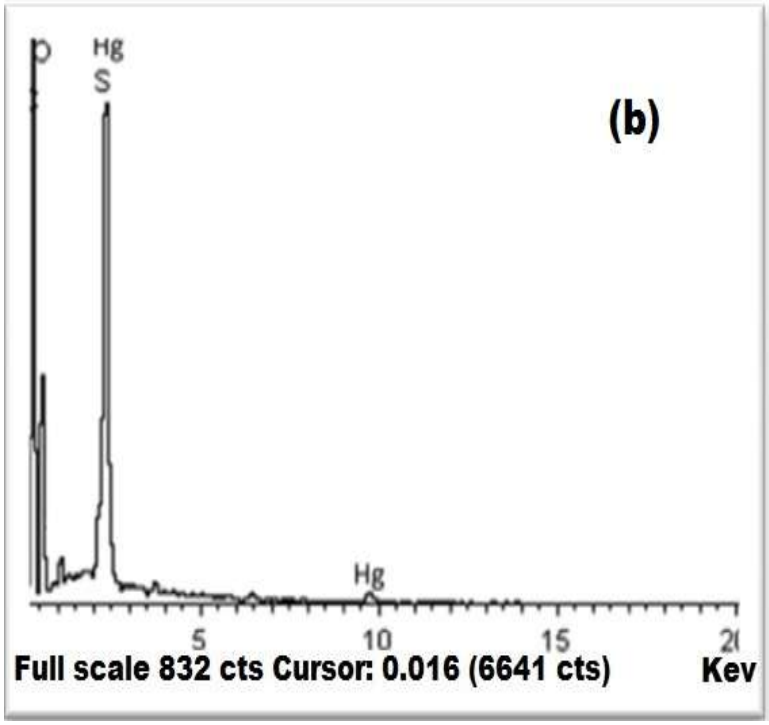
Hg
S
(b)
Hg
5
10
15
Full scale 832 cts Cursor: 0.016 (6641 cts)
Kev

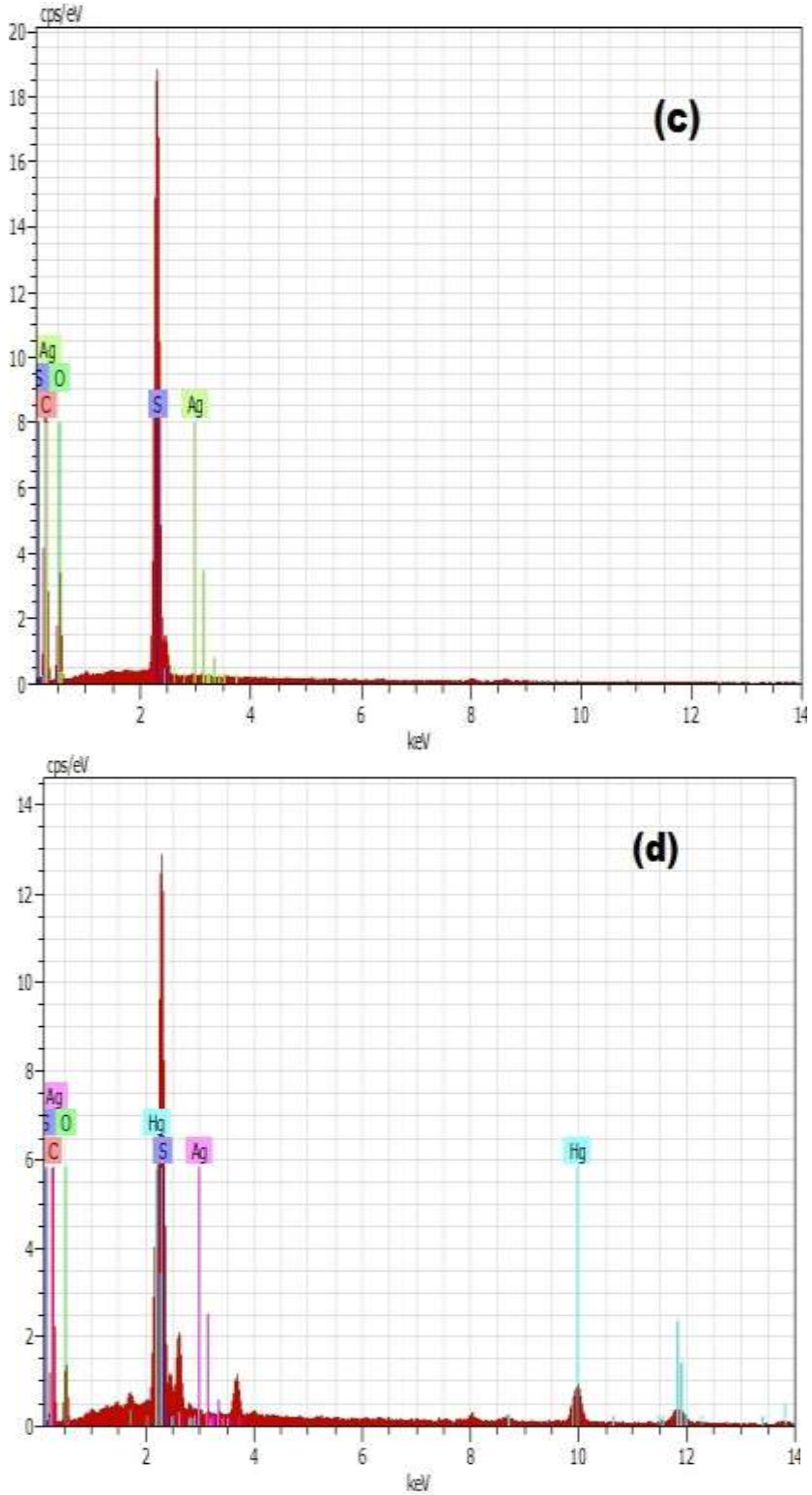

Fig.4 EDX spectra of free (a and c) & Hg^{2+} loaded (b and d) RFR & RFR-AgNPs

The SEM-EDAX spectrum of free and Hg (II) loaded adsorbent are shown in fig 4a, 4b, 4c and 4d. The presence of Hg (II) peaks in the spectrum after adsorption confirms the adsorption of Hg (II) onto RFR and RFR-AgNPs.

The TGA (Fig.5a and 5b) & DTA (Fig.6a and 6b) analysis of the free and Hg^{2+} loaded RFR-AgNPs are indicated a shift in temperature dominant peaks correlated with the loaded metal. This shift in the temperature evidences that the metal binding process occurring at the surface of RFR-AgNPs.

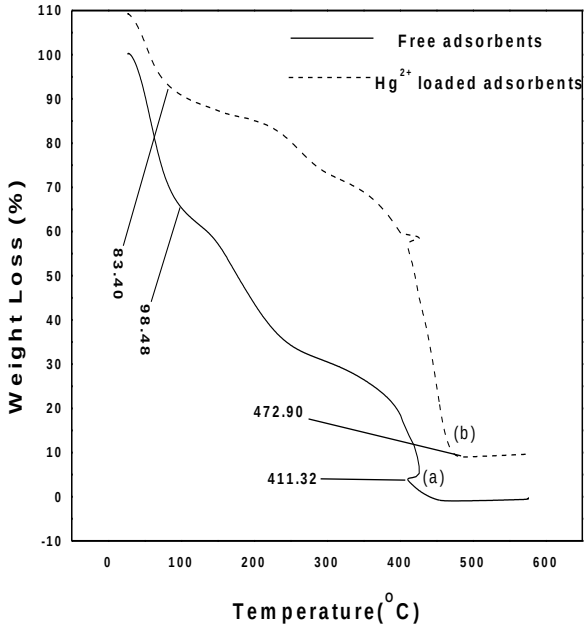

Fig.5. TGA analysis of free (a) and Hg^{2+} loaded (b) RFR-AgNPs

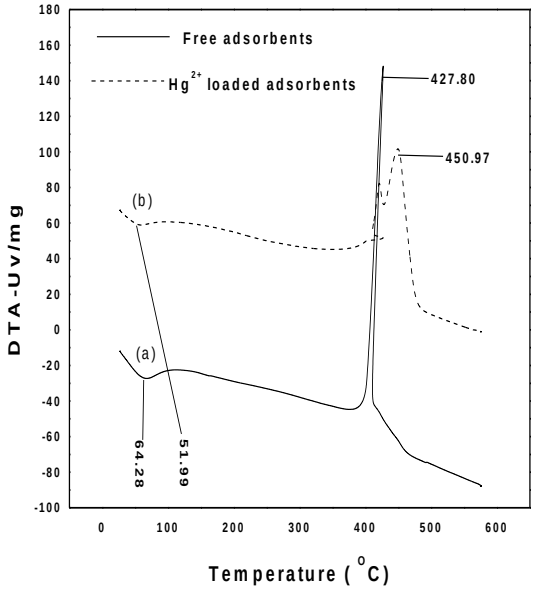

Fig.6. DTA analysis of free (a) and Hg^{2+} loaded (b) RFR-AgNPs

B. Effect of contact time and initial Hg (II) concentration on the Hg^{2+} retention:

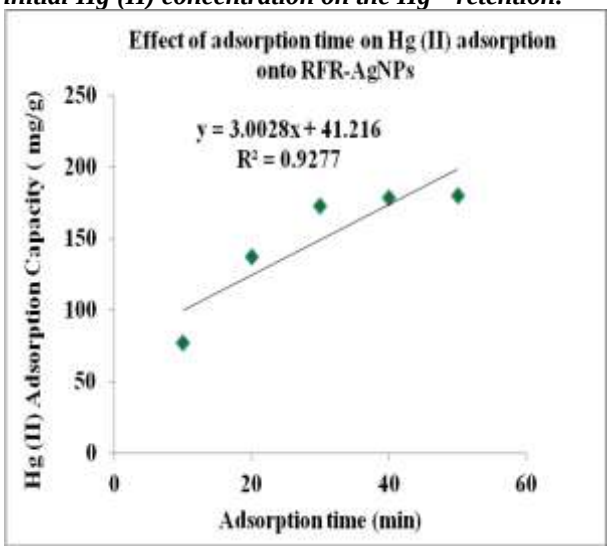

Fig.7 Effect of adsorption time on Hg (II) adsorption onto RFR-AgNPs

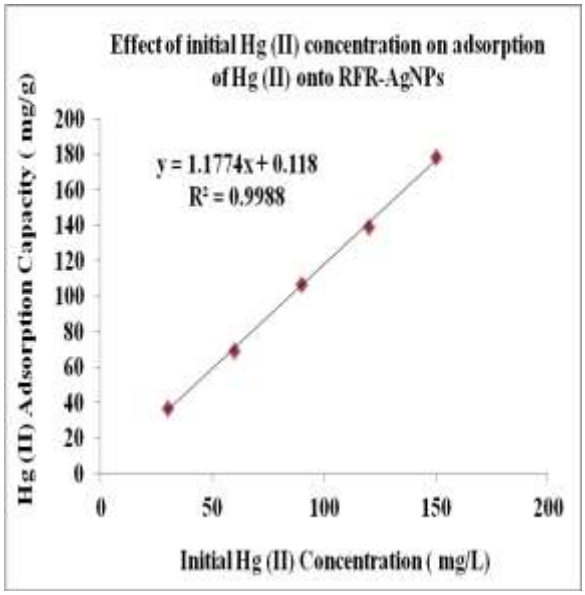

Fig.8 Effect of Hg (II) concentration on adsorption of Hg (II) onto RFR-AgNPs

A cycle of agitation time analyzes for Hg^{2+} ions have been performed with metal ion concentration 150 mg/L at 303 K and followed by agitated with 200 rpm. Fig. 7 demonstrates that the amount of the adsorbed Hg^{2+} ions on RFR-AgNPs increases with time. The shakeup time required to attain equilibrium was 40min.The elementary adsorption rate was extremely rapid due to the existence of more number of adsorbent sites existing for Hg^{2+} removal from aqueous solution. Whereas the remaining vacant surface areas decreases, the adsorption rate delayed due to the progress of repulsive forces between the Hg^{2+} ions on the solid surface and in the liquid phase. The adsorption capacities (q_e) increase with the increase in initial concentration from 50 to 150 mg/L was indicated in Fig.8 owing to the enhance in driving force attributable to concentration gradient developed between the bulk solution and surface of the RFR-AgNPs. Hence the built-up RFR-AgNPs can be proficiently applied for the extraction of high concentration of heavy metals from wastewater [20].

C. Adsorption isotherms

These are significant for evaluate the adsorption process since a unit operation. They give adsorption capacity below analyzed terms as well as provide an idea regarding adsorption mechanism along with feature of adsorption. Freundlich and langmuir adsorption replicas are the almost commonly utilized equations in the literature, showing the nonlinear correlation between adsorbed metal ion on the adsorbent and metal ion in the solution.

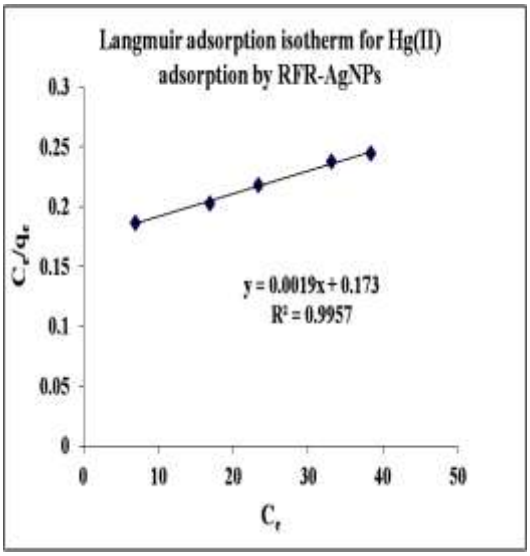

Fig.9 Langmuir adsorption isotherm for Hg(II) adsorption by RFR-AgNPs

The Langmuir adsorption model states that the solid surface has a fixed number of regular sites and they are dynamically identical and a monolayer is formed as the solid surface achieves saturation. The Langmuir isotherm model is uttered with the following equation [21]:

$$\textbf{Langmuir isotherm} \quad : (C_e / q_e) = (1 / Q_o b) + (C_e / Q_o) \qquad \text{-------- (3)}$$

Where $\mathbf{q_e}$ (mg g^{-1}) is the adsorbed amount of Hg (II) at equilibrium, $\mathbf{C_e}$ (mg L^{-1}) is the equilibrium concentration of Hg (II), $\mathbf{Q_o}$ (mg g^{-1}) and b (g L^{-1}) are Langmuir constants related to

Table 3 Adsorption isotherm factors for the Hg (II) retention

Metal ion	Langmuir				Freundlich		
	Q_o (mg/g)	b (g/l)	$R_L=1/1+Q_ob$	R^2	n	K_F	R^2
Hg (II)	526.32	0.0109	0.1474	0.9957	1.1069	6.0981	0.9829

adsorption capacity and energy of adsorption. The graph $\mathbf{C_e/q_e}$ against $\mathbf{C_e}$ (Fig.9) provided a straight line outlooking the soundness of Langmuir isotherm. The values of $\mathbf{Q_o}$ and b are found from slope and intercept of the plot and are stated in Table 3. The vital individualities of the Langmuir isotherm can be articulated through the dimensionless seperation factor $\mathbf{R_L}$. The magnitude of R_L decides the nature as well as feasibility of the adsorption process with the following equation.

$$\mathbf{R_L = 1/ (1+bQ_o)} \quad \text{---------- (4)}$$

When RL = 0, the sorption is irreversible; When RL < 1, the sorption is favorable; When RL > 1, the sorption is unfavorable and When RL = 1, the sorption is linear. RL values in Table 3 indicate that the adsorption process onto RFR-AgNPs is favorable.

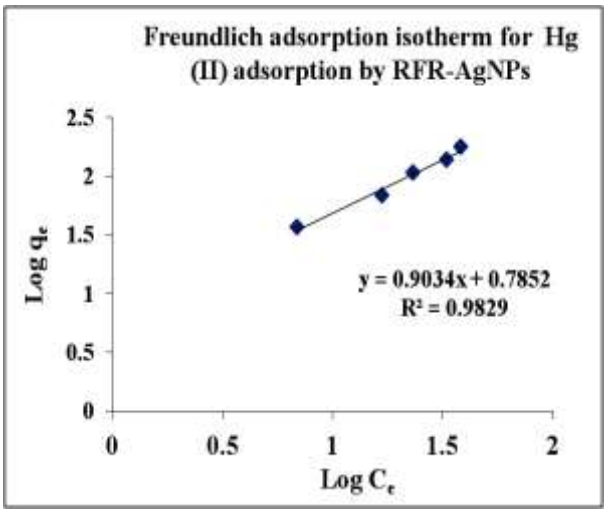

Fig.10 Freundlich adsorption isotherm for Hg (II) adsorption by RFR-AgNPs

Freundlich isotherm is an empirical equation obtained since the adsorption on a heterogeneous surface indicating that binding sites are not equivalent and the adsorbent has a surface with a non-uniform dispersion of heat of adsorption. The Freundlich isotherm model [22] in linear forms are stated as:

Freundlich isotherm : $\log q_e = \log K_F + (1/n) \log C_e$ ------- (5)

Where K_F (mg g^{-1}) is the Freundlich constant and 'n' the freundlich exponent. Where q_e (mg g^{-1}) is the adsorbed amount of Hg (II) at equilibrium and C_e (mg L^{-1}) is the equilibrium concentration of Hg (II). The entire values are calculated and indicated in Table 3 from Fig.10. The n value (1.1069) indicated that the RFR-AgNPs is superior adsorbent for the Hg (II) retention from aqueous medium. Then the R^2 value of the langmuir model are higher than that of the Freundlich model for RFR-AgNPs sample. Hence, it can be resolved that Freundlich model marvelously interpreted the extraction of Hg (II) on RFR-AgNPs adsorbents.

D. Reaction and Diffusion-base kinetic models

This is familiar that the result of kinetics in batch mode is essential for planning of adsorption schemes as well as clearly elucidate the rate of chemical reactions. This study ia also

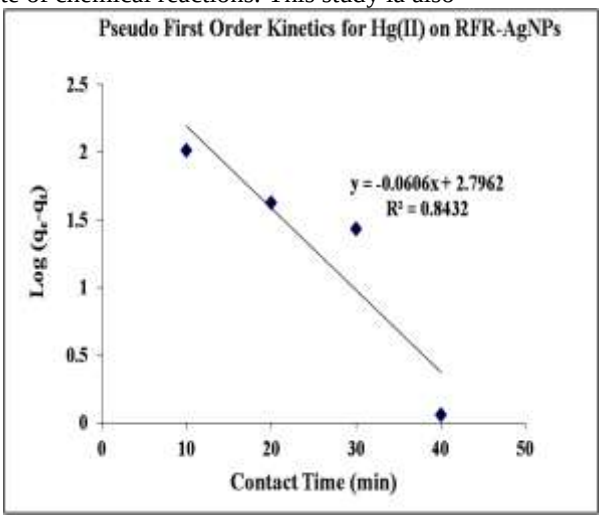

Fig.11 Pseudo First Order Kinetics for Hg (II) on RFR-AgNPs

used to evaluate the efficiency of the adsorbent. So as to study the rate constant and mechanism of adsorption for the Hg^{2+} ions was calculated with the Lagergren pseudo-first order equation which is generally stated as [23].

$\text{Log } (q_e - q_t) = \log q_e - [K_1 / 2.303] t$ ---------- (6)

Where $\mathbf{K_1}$ is the pseudo-first-order rate constant (min^{-1}) and $\mathbf{q_e}$ ($mg\ g^{-1}$) is the adsorption capacity at equilibrium and $\mathbf{q_t}$ ($mg\ g^{-1}$) is the adsorbed amount of metal ion after time t (min). The all values are calculated from Fig.11 and are presented in Table.4.

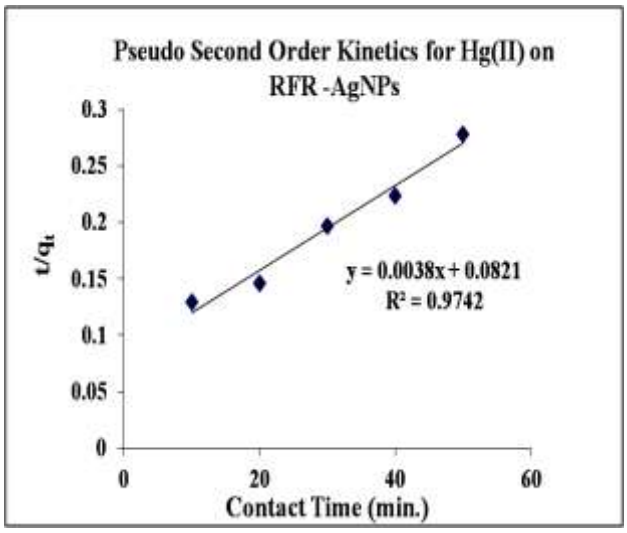

Fig.12 Pseudo Second Order Kinetics for Hg (II) on RFR-AgNPs

Table 4 Kinetic factors for the Hg (II) retention

Metal ion	Experimental q_e (mg/g)	Pseudo-I-Order constants			Pseudo-II-Order constants		
		q_e (mg/g)	K_1 (min^1)	R^2	q_e (mg/g)	K_2 (g/mg/min)	R^2
Hg^{2+}	178.60	625.46	0.1396	0.8432	263.16	1.76×10^{-4}	0.9742

The pseudo second-order kinetic model into linear form and based on chemical adsorption can be expressed as [24]:

$$t / q_t = 1/ K_2 q_e^2 + t/q_e \quad \text{---------- (7)}$$

Where $\mathbf{K_2}$ is the rate constant of second order adsorption (g/mg/min). The q_e and K_2 values were calculated of the slope and intercept peak of (t/qt) vs t plot (Fig.12) and tabulated in Table.4. The R^2 value of the pseudo-first order kinetic model was 0.8432, it indicates impoverished correlation of the this model for RFR-AgNPs and also its experimental value (qe) is deprived harmony with the theoretical value of pseudo-first-order kinetic model. While, Pseudo-second-order kinetic model demonstrates superior R^2 value as 0.9742. Moreover, the much better correlation between calculated and experimental $\mathbf{q_e}$ values noted that the adsorption system followed the pseudo second-order kinetic model. This outcome signifies that the adsorption of Hg^{2+} onto RFR-AgNPs controlled via chemisorption.

The intraparticle diffusion (k_{id}) rate constant was originated [25] for more assess the adsorption process. Fig.13 demonstrates that the plot control three regions reporting the mass transfer on the RFR-AgNPs. This equation can be expressed as

$$q_t = K_{id}\, t^{1/2} + C \quad \text{---------- (8)}$$

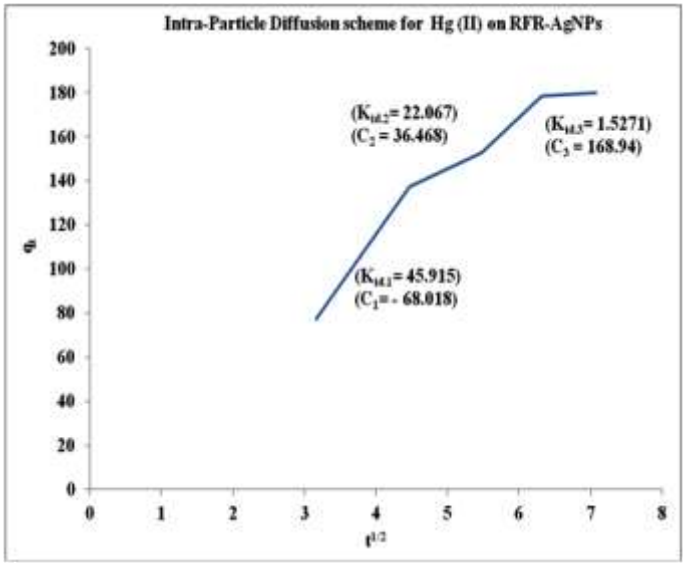

Fig.13 Intra-Particle Diffusion for Hg (II) on RFR-AgNPs

Table 5 Intraparticle diffusion factors for the Hg (II) retention

Metal ion	Intraparticle diffusion rate (g mg^{-1} $min^{-1/2}$)			Film thickness		
	$K_{id.1}$	$K_{id.2}$	$K_{id.3}$	C_1	C_2	C_3
Hg (II)	**45.915**	**22.067**	**1.5271**	**-68.018**	**36.468**	**168.94**

Where $\mathbf{q_t}$ is the adsorption capacity at any time t and $\mathbf{K_{id}}$ is the intra particle diffusion rate constant and C is the film thickness. The intraparticle diffusion constants could be determined from the slop of the plots. The $K_{id.1}$, $K_{id.2}$ and $K_{id.3}$ and C_1, C_2 and C_3 which utter the diffusion rates and film thickness values of the diverse points in adsorption process are evaluated from the slop of the schemes and tabulated in Table 5. The order of rate of adsoption and value of film thichness is $K_{id.1} > K_{id.2} > K_{id.3}$ and $C_1 < C_2 < C_3$. The Hg^{2+} ion experienced initially a sharp- gradient level, subsequently the falling gradient and the later level until equilibrium. The primary sharp-gradient stage is the direct diffusion level ($K_{id.1}$ = 45.915), through which a bulky amount of mercury ions were quickly adsorbed through the external plane of the adsorbent. As soon as the adsorption of external plane attained saturation, mercury ions penetrated into the pores of the adsorbent as well as were adsorbed through the internal plane of the nanopores. By the mercury ions penetrating into the pores, the diffusion hostility enhanced as well as resulting to lessen of the rate of diffusion ($K_{id.2}$ = 22.067). By the quick decrease of the mercury ions concentration, the rate of intraparticle diffusion progressively delayed as well as lastly attained the equilibrium point ($k_{id.3}$ = 1.5271). As well, the values of film thickness of the adsorbent were increased in every stages due to the increase of mercury ions concentration over the adsorbent in each stages (C_1 = -68.018, C_2 = 36.468 and C_2 = 168.94) [26].

***E. Adsorption thermodynamics**:*

Thermodynamic parameters like enthalpy change (ΔH^O), free energy change (ΔG^O) and entropy change (ΔS^O) were evaluated as of the difference of the thermodynamic equilibrium constant (K_C) at various temperatures (303K-33K). The K_C values were found out with the following equation:

$$\mathbf{K_C = C_{ad}\,(solid) / C_e\,(solution)} \quad \text{---------- (9)}$$

C_{ad} is the amount of metal (mg) adsorbed on the adsorbent per liter (L) of the solution at equilibrium, and C_e is the equilibrium concentration (mg L^{-1}) of the metal in the solution. The ΔH^O and ΔS^O values were determined since the slope and intercept of Van't Hoff scheme log K_C versus 1/T (Fig.14).

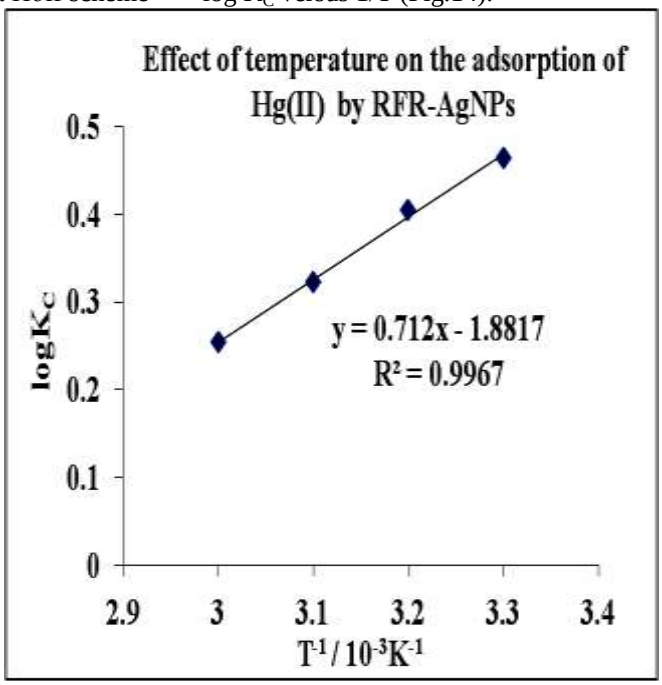

Fig.14 Effect of temperature on the adsorption of Hg (II) by RFR-AgNPs

Log K_C = - [ΔH^O / 2.303 RT] + (ΔS^O / 2.303R) --------- (10)

Table 6 Thermodynamic factors for the Hg (II) retention

Temperature	-ΔG^o (kJ mol^{-1})				-ΔS^O (J $mol^{-1}K^{-1}$)	-ΔH^O (kJ mol^{-1})
	30°C	40°C	50°C	60°C		
Hg (II)	2690	2422	1996	1616	36.03	13.63

Where T is the absolute temperature (K) and R is universal gas constant (8.314 J mol^{-1} K^{-1}). The standard free energy change (ΔG^O) of the adsorption was evaluated through the following equation:

ΔG^O = -2.303 RT log K_C ---------- (11)

The determined all values were tabulated in Table.6. The small values of ΔH^O recommended that the electrostatic interaction and ion exchange is accountable for the adsorption of Hg (II) on RFR-AgNPs. The nrgative value of the enthalpy change (ΔH^O = - 13.63 kJ mol^{-1}) shows that the adsorption is exothermic. The Gibbs free energy change values were observed as negative, which suggested the feasibility and spontaneity of the adsorption process between Hg^{2+} and RFR-AgNPs . The negative entropy change (ΔS^O = - 36.03 kJ mol^{-1}) value represents to decrease in the degree of freedom of the adsorbed groups [27].

F. Column studies:

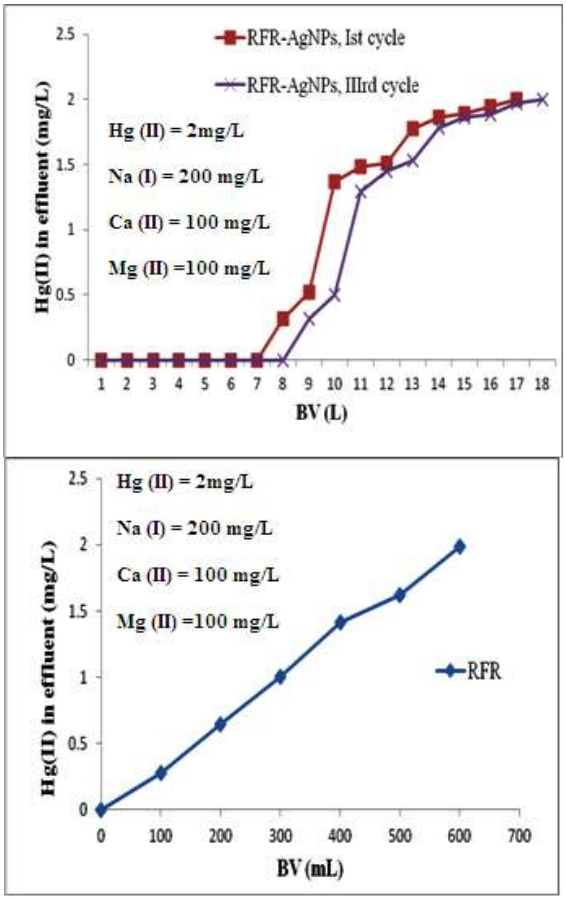

Fig.15 Comparison of breakthrough curves of Hg (II) adsorption by RFR-AgNPs and RFR.

The breakthrough curve is especially main features for finding out the process and the dynamic reaction of adsorption in a fixed-bed column [28]. The uninterrupted adsorption of Hg^{2+}on RFR and RFR-AgNPs was studied in the presence of competing ions like Na^{+}, Ca^{2+} and Mg^{2+} by a research laboratory scale in a fixed-bed. The breakthrough time and exhaustion time

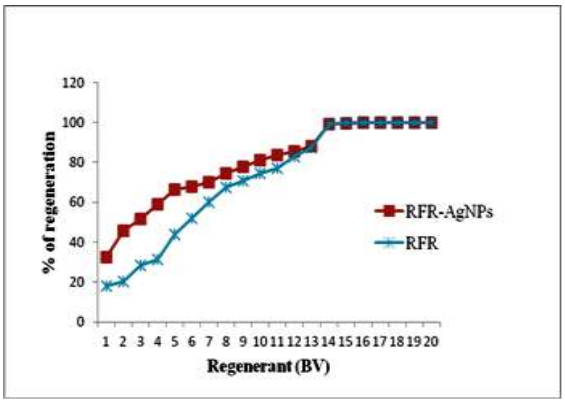

Fig.16 A column regeneration capacity of the RFR-AgNPs and RFR.

For Hg^{2+} ion was found [29] and shown in Fig.15 and the RFR was also needed for reference. It was indicated that the Hg (II) breaks through rapidly on the RFR due to its scanty selectivity towards mercury and the effective treatment volume is almost 600 bed volumes (BV). On the contrary, appropriate breakthrough results were determined for RFR-AgNPs as about 8000BV in identical conditions due to the immobilized negatively charged

sulfonic acid groups bound to polymer matrix would significantly improved the permeation and preconcentration of the Hg (II) from aqueous media to interior plane of the polymer [30] as well as successively make favorable conditions for Hg (II) retention by AgNPs. This effect is called as potential donnan membrane effect. Besides, Hg (II) can be selectively withdrawn by AgNPs particles by outer-sphere complexation of Hg (II) with AgNPs [31].The mercury concentration in the effluent reduced considerably from 2 less than 0.001mg/L, this limit was allowed according to WHO and Environmental Bureau of Investigation. As the exhausted RFR and RFR-AgNPs column was regenerated by a 10% (w/w) NaCl solution and the results are shown in Fig.16. It was shown that the 15-20BV regenerates can be efficiently regenerated the preloaded mercury from the resin. Also, we carried out a continuous adsorption– regeneration cycle runs for RFR-AgNPs bed-column to confirm its feasibility for future application. The imbrications of mercury breakthrough curves for the 1st and 3rd cycle confirmed that RFR-AgNPs can be utilized for repetitive use without noticeable capacity loss after regeneration by 10% (w/w) NaCl solution. Note down that the dynamic adsorption capacities of RFR-AgNPs and RFR column towards mercury with opposing ions (Na^{+}, Ca^{2+}, and Mg^{2+}) was around 171.68 and 153.104 mgg^{-1}.

G. Comparison of maximum adsorption capacity of RFR-AgNPs adsorbent with some other adsorbents

As the Freundlich adsoption replica does not illustrate the saturation demeanor of the adsorbents, the Langmuir constant (Q_O), signifies the monolayer saturation at equilibrium. The adsorption capacity value (Q_O) found for Hg (II) in this study is 526.32 mg/g. The variations of metal intake were caused by the properties of adsorbents like structure, functional groups and surface area. The adsorption capacities of the RFR-AgNPs and other adsorbents for the removal of Hg^{2+} from aqueous solution or wastewater were mentioned in Table 7 which showed that the adsorption capacity of the RFR-AgNPs dealt in the present work was higher than the other literature reported adsorbents [32-38].

H. In vitro antibacterial screening

The bacterial inhibiting efficiency of the silver nanoparticles proved to be of great interest for the prevention of adherence and proliferation activities of some bacteria on the materials

Table 7 Relationship of adsorption capacities of several adsorbents with RFR-AgNPs adsorbent

Adsorbent	Hg (II)	Reference
polyacrylamide-grafted iron(III) oxide	155	[32]
cross-linked magnetic chitosan-phenyl thiourea resin	135	[33]
Ethylenediamine modified peanut shells	30.78	[34]
Rice straw	27.7	[35]
Thiol containing polymer encapsulated magnetic Nanoparticles	16.02	[36]
Carboxyl banana stem	88.98	[37]
Triethylenetetramine modified polystyrene resin	344.8	[38]
RFR-AgNPs	**526.32**	**Present work**

surface [39-40]. Further, bacterial invasion was one of the undisputed functions of their protective role [41]. This showed their presence in constitutive antibacterial agents in response to bacterial attack. Hence, we putforth the in vitro antibacterial measurements of our RFR-AgNPs, RFR and AgNPs against microorganisms which cause water-

borne diseases viz., Escherichia coli, Salmonella typhi (Gram-negative), Bacillus subtilis and Staphylococcus aureus (Gram-positive) [42]. Escherichia coli and Salmonella typhi were the most common bacteria among all. The results of qualitative antibacterial paper disk method tests illustrated the significant efficiency of RFR-AgNPs on all the microorganisms compared to others. The average inhibition zones observed for our products listed in Table 8 indicated that after 48 h of incubation, the zones of inhibition for RFR-AgNPs composite versus bacteria were significantly outlined (12 – 15 mm).

Table 8 In vitro antimicrobial investigation of the RFR-AgNPs

Synthesized Compounds	Antibacterial activity			
	B. Subtilis	S. Aureus	S. typhi	E. coli
AgNPs	+++	+	+++	++
RFR	++	+	+	++
RFR-AgNPs	+++	+++	++++	++++
Ciprofloxacin	++++	++++	++++	++++
Deionized water	–	–	–	–

(–, no inhibition (<3 mm); +, clear zone of 3-6 mm; ++, clear zone of 6-9 mm; +++, clear zone of 9-12 mm; ++++, clear zone of 12-15 mm)

It can be seen that the lower inhibition zone was obtained in the case of Bacillus subtilis and Staphylococcus aureus (about 9 mm), whereas the inhibition halos measured for Escherichia coli and Salmonella typhi were higher suggesting that for these situations, the silver composite showed superior bactericidal activities than its precessor. This proved that the existence of silver nanoparticles impregnated within the polymeric matrix demonstrated to be effective in inhibiting bacterial growth. Although the exact role of silver nanoparticles in the immediate surrounding of the composite film is not very clear, the literature data explain the huge zones of inhibition produced by other films through the same mechanism of release of silver, which implies a oxidation reaction at the nanoparticle surface and diffusion of the silver ions thus causing structural changes and finally, bacterial death [43]. In agreement with these results, the above hybrid composites manifest a real potential for antimicrobial coatings in a wide variety of bioapplications. Ciprofloxacin acts as the standard while deionized water as a negative control which doesnot involve in any significant inhibition. Here, the bacterial activity of RFR-AgNPs may be due to their interaction with protein, which leads to the inactivation of protein and direct interaction with DNA. This interaction generates the mutation and stops the replication ability of DNA. Further, these nanoproducts can also undergo a cell wall passage easily due to their smaller size, thus inducing the cell lysis. It is also believed that the RFR-AgNPs after penetration into the microbes inactivate their cellular proteins/enzymes by possibly interacting with the DNA leading to bacterial cell death [44]. Besides, the results realized from this investigation show a good harmony with the antibacterial outlook of our RFR-AgNPs.

IV. Conclusion

In the recent study prepared polymer supported silver nanopartcles (RFR-AgNPs) exhibited a selective adsorbent for Hg^{2+} retention from aqueous medium and waste water. As compared to RFR, RFR-AgNPs showed more favorable Hg^{2+} adsorption from aqueous media in the presence of competing ions due to the potential donnan membrane effect exerted by loading AgNPs. The pseudo second-order replica indicates a superior fit with the experimental data than the pseudo first-order replica. The adsorption process can be obviously explained with intraparticle diffusion model as well as the the order of adsoption rate and film thichness value is $K_{id.1} > K_{id.2} > K_{id.3}$ and $C_1 < C_2 < C_3$. The adsorption of Hg^{2+} on RFR-AgNPs fitted well with Langmuir adsorption isotherm. The maximal adsorption capacity was 526.32 mg/g at 303 K according to the Langmuir adsorption isotherm. Thermodynamic parameters showed that the ion-exchange process is exothermic, feasible and spontaneous. Fixed-bed column consequences demonstrated that mercury retention onto a RFR-AgNPs could answer in a obvious reduce of this toxic metal from 2 less than 0.001mg/L. Besides, the spent RFR-AgNPs beads are able to readily regenerated by 10% (w/w) NaCl solution for frequent use with no any considerable capacity loss. Additionally, the incorporation of silver particles into RFR present their antibacterial properties against water-borne diseases causing

S. aureus, S. typhi, E. coli and B. Subtilis. Therefore, these materials have great potential for utilization in the fabrication of antibacterial coatings and textiles. These results indicated that the RFR-AgNPs can be applied in prevention and treatment of diseases caused by microbes and mercury retention for environmental applications.

References

[1] Zhang, F.S.; Nriagu, J.O.; Itoh, H. Mercury removal from water using activated carbons derived from organic sewage sludge. Water Res. 2005, 39, 389–395.

[2] Huang, Z.H.; Zheng, X.; Lv, W. ; Wang, M.; Yang, Q.H.; Kang, F. Adsorption of lead (II) ions from aqueous solution on low-temperature exfoliated grapheme nano sheets. Langmuir. 2011, 27, 7558–7562.

[3] Siva, S.; Sameem, S.M.; Sudharsan, S.; Sayeekannan, R. Synthesis, Characterization and Application of Zero-Valent Silver nano Adsorbents. IJIRSET.2013, 2, 8023-8037.

[4] Mayo, J.T.; Yavuz, C.; Yean, S.; Cong, L.; Shipley, H.; Yu, W. The effect of nano crystalline magnetite size on arsenic removal. Sci Technol Adv Mater. 2007, 8, 71–75.

[5] Gu, Z.M.; Fang, J.; Deng, B.L. Preparation and evaluation of GAC-based iron-containing adsorbents for arsenic removal. Environ Sci Technol. 2005, 39, 833-843.

[6] Yuchi, A.; Ogiso, A.; Muranaka, S. Niwa, T. Preconcentration of phosphate and arsenate at sub-ng.ml−1 level with a chelating polymer–gel loaded with zirconium (IV). Anal Chim Acta. 2003, 494, 81–86.

[7] Siva, S; Sudharsan, S; Sayee Kannan, R. Synthesis, characterization and ion-exchange properties of novel hybrid polymer nanocomposites for selective and effective mercury (II) removal†. RSC Adv. 2015, 5, 79665–79678.

[8] Siva, S.; Sudharsan, S.; SayeeKannan, R. Selective Co (II) removal from aqueous media by immobilizing the silver nanoparticles within a polymer-matrix through formaldehyde cross linking agent. RSC Adv. 2015, 5, 23340–23349.

[9] Sondia, I.; Salopek-Sondi, B. Silver nanoparticles as antimicrobial agent: a case study on E. coli as a model for gram-negative bacteria. J. Colloid Interf. Sci. 2004, 275, 177-182.

[10] Elechiguerra, J.; Burt, J.; Morones, J.; Camacho-Bragado, A.; Gao, X.; Lara, H. Yacaman, M. Interaction of silver nanoparticles with HIV-1. J. Nanobiotechnol.2005, 3, 3-6.

[11] Sharma, V.K.; Yngard, R.A.; Lin, Y. Silver nanoparticles: green synthesis and their antimicrobial activities. Adv. Colloid Interf Sci. 2009, 145, 83-96.

[12] S. Siva, S. M. Sameem, S. Sudharsan and R. Sayee Kannan, Green, effective biological route for the synthesis of silver nanoparticles using Cyperus rotundus grass extracts, Int. J. Curr. Res. 2014, 6, 4532–4538.

[13] Vasudevan, P.; Sharma, N.L.N. Composite cation exchangers. J. Appl. Poly. Sci.1979, 23, 1443-1448.

[14] Metwally, M.S.; Metwally, N.E.; Samy, T.M. Synthesis and studies of Egyptian bagasse pith phenol formaldehyde cationic exchangers. J. Appl. Poly. Sci. 1994, 52, 61-67.

[15] Natarajan, M.; Krishnamoorthy, S. Studies on p-cresol-formaldehyde cationic resins substituted by coconut shell carbon. Res. Ind.1993, 38, 278-282.

[16] Bassett, G.H.; Jeffery, J.; Mendham, J.; Denney, R.C. Vogel's Text Book of Quantitative Chemical Analysis, fifth Ed, Longman, London, 1989.

[17] Chandra, S.; Gupta, L.K. EPR, IR and electronic spectral studies on Mn(II), Co(II), Ni(II) and Cu(II) complexes with a new 22-membered azamacrocyclic [N4] ligand. Spectrochim. Acta A. 2004, 60, 1751-1761.

[18] Prathna, T.C.; Chandrasekaran, N.; Raichur, A.M. Mukherjee, A. Biomimetic synthesis of silver nanoparticles by citrus limon aqueous extract and theoretical prediction of particle size Colloids Surf. B: Biointerfaces. 2011, 8, 152-159.

[19] Srivastava, V.C.; Mall, I.D.; Mishra, I.M. Characterization of mesoporous rice husk ash (RHA) and adsorption kinetics of metal ions from aqueous solution onto RHA. J.Hazard.Mater. 2006, 314, 257-267.

[20] Acemioglu, B. Batch kinetic study of sorption of methylene blue by perlite. Chem. Eng. J. 2005, 106, 73–81.

[21] Aksu, Z.; Balibek, E. Chromium (VI) biosorption by dried Rhizopus arrhizus: effect of salt (NaCl) concentration on equilibrium and kinetic parameters. J. Hazard. Mater. 2007, 145, 210–220.

[22] Dang, V.B.H. ; Doan, H.D.; Dang-Vu T.; Lohi, A. Equilibrium and kinetics of biosorption of cadmium (II) and copper (II) ions by wheat straw. Bioresour. Technol. 2009, 100, 211–219.

[23] Barassi, G.; Valdes, A.; Araneda, C.; Basualto, C.; Sapag, J.; Tapia, C.; Valenzuela, F. Cr (VI) sorption behavior from aqueous solutions onto polymeric microcapsules containing a long-chain quaternary ammonium salt: kinetics and thermodynamics analysis. J. Hazard. Mater. 2009, 172, 262–268.

[24] Anirudhan, T.S.; Jalajamony, S.; Suchithra, P.S. Improved performance of a cellulose-based anion exchanger with tertiary amine functionality for the adsorption of chromium(VI) from aqueous solutions. Colloids Surf. A: Physicochem. Eng. Aspec. 2009, 335, 107–113.

[25] Asfour, H.M.; Nassar, M.M.; Fadali, O.A.; El-Geundi, M.S. Colour removal from textile effluents using hardwood saw dust as an adsorbent. J. Chem. Technol. Biotechnol. 1985, 35, 28–35.

[26] Sun, Q.Y.; Yang, L.Z. The adsorption of basic dyes from aqueous solution on modified peat-resin particle. Water Res. 2003, 37, 1535–1544.

[27] Vasiliu, S.; Bunia, I.; Racovita, S.; Neagu, V. Adsorption of cefotaxime sodium salton polymer coated ion exchange resin microparticles: kinetics, equilibrium andthermodynamic studies. Carbohydrate Polymers. 2011, 85, 376–387.

[28] Gupta, V.K.; Mittal, A.; Gajbe, V.; Mittal, J. Removal and recovery of the hazardous azo dye acid orange 7 through adsorption over waste materials: Bottom ash and de-oiled soya, Ind. Eng. Chem. Res. 2006, 45, 1446–1453.

[29] Gupta, V.K.; Rastogi, A.; Nayak, A. Adsorption studies on the removal of hexavalent chromium from aqueous solution using a low cost fertilizer industry waste material. J. Colloid Interf. Sci. 2010, 342, 135–141.

[30] Pan, B.C.; Zhang, Q.R.; Zhang, W.M.; Pan, B.J.; Du, W.; Lv, L. Highly effective removal of heavy metals by polymer-based zirconium phosphate. A case study of lead ion. J Colloid Interf Sci. 2007, 310, 99-105.

[31] Villalobos, M.; Bargar, J.; Sposito, G. Mechanisms of Pb (II) sorption on a biogenic manganese oxide. Environ Sci Technol. 2005, 39, 569–576.
[32] Manju, G.N.; Krishnan, K.A.; Vinod, V.P.; Anirudhan, T.S. An investigation into the sorption of heavy metals from wastewaters by polyacrylamide-grafted iron(III) oxide. J. Hazard. Mater. 2002, 91, 221–238.
[33] Monier, M.; Abdel-Latif, D.A. Preparation of cross-linked magnetic chitosan-phenylthiourea resin for adsorption of Hg (II), Cd (II) and Zn (II) ions from aqueous solutions. J. Hazard. Mater. 2012, 209, 240– 249.
[34] Yong, L.; Xiaomei, S. Buhai, L. Adsorption of Hg^{2+} and Cd^{2+} by ethylenediamine modified peanut shells. Carbohydr. Polym. 2010, 81, 335–339.
[35] Rocha, C.G.; Zaia, D.A.M.; Da Silva Alfaya, R.V.; Da Silva Alfaya, A.A. Use of rice straw as biosorbent for removal of Cu(II), Zn(II), Cd(II) and Hg(II) ions in industrial effluents. J. Hazard. Mater. 2009, 166, 383–388.
[36] Shin, S.; Jang, J.; Thiol containing polymer encapsulated magnetic nanoparticles as reusable and efficiently separable adsorbent for heavy metal ions. Chem. Commun. 2007, 4230–4232.
[37] Anirudhan,T.S.; Senan, P.; Unnithan M R, 2007. Sorptive potential of a cationic exchange resin of carboxyl banana stem for mercury (II) from aqueous solutions. Separation and Purification Technology, 2007, 52, 512–519.
[38] Chunhua, X.; Caiping, Y.; Synthesis, characterization and application of triethylenetetramine modified polystyrene resin in removal of mercury, cadmium and lead from aqueous solutions. Chem. Eng. J.. 2009, 155, 844–850.
[39] Tran, H.V.; Tran, L. D.; Ba, C. T.; Vu, H. D.; Nguyen, T. N.; Pham, D. G.; Nguyen, P. X. Synthesis, characterization, antibacterial and antiproliferative activities of monodisperse chitosan- based silver nanoparticles. Colloids Surf. A: Physicochem. Eng. Aspects. 2010, 360, 32-40.
[40] Saha, S.; Sarkar, J.; Chattopadhyay, D.; Patra, S.; Chakraborty, A.; Acharya, K. Production of silver nanoparticles by a phytopathogenic fungus Bipolaris nodulosa and its antimicrobial activity. Digest J. Nanomater. Biostruct. 2010, 5, 887-895.
[41] Yadav, S.C.; Kumari, A.; Ramdhan, Y. Development of peptide and protein nanotherapeutics by nanoencapsulation and nanobioconjugation. Peptides. 2011, 32, 173-187.
[42] Campoccia, D.; Montanaro, L.; Arciola, C.R. The significance of infection related to orthopedic devices and issues of antibiotic resistance. Biomaterials.2006, 27, 2331-2339.
[43] Kuegler, R.; Bouloussa, O.; Rondelez, F. Evidence of a charge-density threshold for optimum efficiency of biocidal cationic surfaces. Microbiology. 2005, 151, 1341-1348.
[44] Shockman, G.D.; Barrett, J.F. Structure, function, and assembly of cell walls of gram-positive bacteria. Annu. Rev. Microbiol. 1983, 37, 501-527.